Synchrotron X-ray-Induced Photoreduction of Ferric Myoglobin Nitrite Crystals Gives the Ferrous Derivative with Retention of the O-Bonded Nitrite Ligand

ARTICLE *in* BIOCHEMISTRY · JULY 2010

Impact Factor: 3.02 · DOI: 10.1021/bi100801g · Source: PubMed

5 AUTHORS, INCLUDING:

George Richter-Addo
University of Oklahoma
125 PUBLICATIONS **2,399** CITATIONS

SEE PROFILE

Published in final edited form as:
Biochemistry. 2010 July 27; 49(29): 5969–5971. doi:10.1021/bi100801g.

Synchrotron X-ray-Induced Photoreduction of Ferric Myoglobin Nitrite Crystals Gives the Ferrous Derivative with Retention of the O-bonded Nitrite Ligand†

Jun Yi[‡], **Allen M. Orville**[§], **John M. Skinner**[§], **Michael J. Skinner**[¶], and **George B. Richter-Addo**[‡,*]

[‡] Department of Chemistry and Biochemistry, University of Oklahoma, 620 Parrington Oval, Norman OK 73019

[§] Biology Department, Brookhaven National Laboratory, Upton, NY 11973-5000

[¶] High School Research Program, Brookhaven National Laboratory, Upton, NY 11973-5000

Abstract

Exposure of a single crystal of the nitrite adduct of ferric myoglobin (Mb) at 100 K to high-intensity synchrotron X-ray radiation resulted in changes in the UV-vis spectrum that can be attributed to reduction of the ferric compound to the ferrous derivative. We employed correlated single-crystal spectroscopy with crystallography to further characterize this photoproduct. The 1.55 Å resolution crystal structure of the photoproduct reveals retention of the O-binding mode of nitrite to the iron center. The data are consistent with the cryogenic generation and trapping, at 100 K, of a ferrous d^6 $Mb^{II}(ONO)$* complex by photoreduction of the ferric precursor crystals using high-intensity X-ray radiation.

Some mammalian proteins such as the heme-containing myoglobin (Mb) can reduce the nitrite anion (NO_2^-; pK_a 3.2) under hypoxic conditions to nitric oxide (NO; eq 1) (1,2) in a process somewhat reminiscent of that employed by denitrifying nitrite reductase (NiR) enzymes.

$$NO_2^- + H^+ + 1e^- \rightarrow NO + OH^- \quad (1)$$

Although this subject area is under active investigation and debate, Gladwin and coworkers have demonstrated that nitrite protects against myocardial infarction in $Mb^{+/+}$ mice, but does not in $Mb^{-/-}$ knockout mice, thus indeed implicating Mb as an in vivo NiR (1).

Clearly, the ability of heme to facilitate nitrite reduction (eq 1) necessitates its presence in the *ferrous* form that can supply the electron needed for this process. We reported the X-ray crystal structure of the related stable *ferric* d^5 Mb-nitrite compound, and showed that the

†This work was supported by the Oklahoma Center for the Advancement of Science and Technology (HR9-081, to GBR-A) and by the Office of Biological and Environmental Research, U.S. Department of Energy and the National Center for Research Resources (2 P41 RR012408, to AMO) of the National Institutes of Health.

*To whom correspondence should be addressed. Phone: (405) 325–6401. Fax: (405) 325–6111. grichteraddo@ou.edu.

SUPPORTING INFORMATION AVAILABLE

X-ray data collection, structure solution and refinement; Movie in avi format showing the single-crystal spectra before and after high-intensity X-ray exposure (for the process described in Fig. 4) as a function of crystal rotation angle. This material is available free of charge via the Internet at http://pubs.acs.org.

nitrite ligand adopted an O-binding mode (i.e., *nitrito*; Fig. 1) (3). A valid criticism of this reported ferric $Mb^{III}(ONO)$ structure is that it may not represent the true binding mode of nitrite to the ferrous Mb just prior to its reduction to NO in vivo. For example, nitrite adopts an N-binding mode in its complex with the ferric Mb H64V mutant (4), and this nitro mode was observed in the X-ray crystal structures of the nitrite adducts of cyt cd_1 NiR (*P. pantotrophus* (5)), sulfite reductase hemoprotein (*E. coli* (6)), and cyt *c* NiR (*W. succinogenes* (7) and *T. nitratireducens* (8)). In contrast, the nitrito mode was observed in the nitrite adduct of ferric human hemoglobin (9).

We were unable, however, and despite several varied attempts, to generate the physiologically important *ferrous* d^6 wild-type Mb-nitrite derivative to determine the nitrite binding mode (3). We have been intrigued by the use of synchrotron X-ray radiation for the generation of electrons in protein crystals (10). We have thus taken advantage of correlated microspectrophotometry and synchrotron X-ray photoreduction techniques to generate and characterize a *ferrous* d^6 Mb-nitrite compound at 100 K.

Single crystals of ferric horse heart $Mb^{III}(ONO)$ at pH 7.4 were generated as previously described (3). The single-crystal UV-vis spectrum of ferric $Mb^{III}(ONO)$ at 100 K is shown in Fig. 2A. Exposure of the crystal to low-intensity X-rays (1.0×10^9 photons/s; ~3% of max. flux) at 100 K at the NSLS that essentially reproduced our "home source" flux (0.7×10^9 photons/s) for 95 mins (calc. total X-ray dose of ~0.046 MGy (11)) resulted in only a very slight change of the spectrum from that of the non-X-ray-exposed crystal (Fig. 2B). In contrast, exposure of the same crystal of ferric $Mb^{III}(ONO)$ to high-intensity X-rays (3×10^{10} photons/s; $\lambda = 1.0$ Å) at a different location along the long, narrow, thin plate morphology of the crystal for 50 min (calc. total X-ray dose ≈ 0.42 MGy) resulted in rapid and dramatic changes in the optical spectrum (Fig. 2C). In particular, the Soret band is red-shifted, and the shape of the bands in the 500–600 nm region undergoes a significant change with the appearance of a relatively intense band at 570 nm. We hypothesized that the changes observed in Fig. 2C (i.e., after exposure of the crystal to high-intensity X-rays) were due to the formation and cryo-trapping of a six-coordinate ferrous d^6 Mb-nitrite derivative (eq 2; * represents X-ray photoreduced species). Our hypothesis

$$Mb^{III}(ONO)+e^- \rightarrow Mb^{II}(ONO/NO_2)^* \quad (2)$$

was based on the fact that the spectral changes observed during exposure of ferric $Mb^{III}(ONO)$ (Fig. 2C) to high-intensity X-rays at 100 K are very similar to those observed by Schlichting (10) and Parak (12) when ferric aquometMb undergoes X-ray photoreduction at cryogenic temperatures to generate the metastable *ferrous* $Mb^{II}(H_2O)$ (eq 3 and Supporting Information).

$$Mb^{III}(H_2O)+e^- \rightarrow Mb^{II}(H_2O) \quad (3)$$

To the best of our knowledge, the UV-vis spectrum of authentic ferrous $Mb^{II}(ONO)$ has not been reported. We note, however, that the UV-vis spectrum of the product generated during photoreduction of ferric $Mb^{III}(ONO)$ (eq 2) is also similar to that of the ferrous six-coordinate $Mb^{II}(CN)$ containing an anionic sixth ligand (13).

We then turned to correlated spectroscopy-crystallography to identify the products from the exposure of crystals of ferric $Mb^{III}(ONO)$ to low- *and* high-intensity X-rays. The UV-vis spectrum of a crystal that had been exposed to "home source" X-ray radiation for data

collection is shown on the left of Fig. 3; the 1.60 Å resolution crystal structure obtained from the diffraction data (flux 0.7×10^9 photons/s; 0.3 mm beam diameter; Table 1) is shown on the right. The spectrum confirms that no significant photoreduction occurred during our home-source X-ray data collection (*c.f.*, Fig. 2B). Figure 4 (left) shows the optical spectra of a ferric $Mb^{III}(ONO)$ crystal before (*solid line*), during (*dashed line*; after image 161; calc. total X-ray dose ≈ 0.45 MGy), and after (*grey line*; after image 365; calc. total X-ray dose ≈ 1.0 MGy) exposure to high-intensity X-rays. Although we collected 365 diffraction image frames (each with 1° oscillation), we only used frames 161–365 for the structure determination because the optical spectra indicated that the product formed during the latter portion of the X-ray exposure was stable. The resulting 1.55 Å resolution crystal structure is shown at the right of Fig. 4. Importantly, the UV-vis spectral changes are consistent with photoreduction to the ferrous d^6 $Mb^{II}(ONO)$* derivative, and the X-ray crystal structure reveals the retention of the O-bound nitrite ligand. This O-binding mode was also observed in a related cobalt-substituted d^6 $Co^{III}Mb(ONO)$ complex (14).

The successful generation of a ferrous $Mb^{II}(ONO)$* complex using high-intensity X-ray radiation may represent a pathway to a non-equilibrium structure in which the O-bonded nitrite is trapped in this position with limited movement in the distal pocket at 100 K. Thus, it may not necessarily represent the true equilibrium structure of the reactive ferrous Mb^{II}-nitrite compound in solution at physiological temperature. Indeed, a similar non-equilibrium retention of the water ligand in X-ray-photoreduced metastable $Mb^{II}(H_2O)$ was obtained at <100 K (12); the complex loses its water ligand at temperatures above 150 K to give the well-characterized five-coordinate deoxy-Mb form obtained by chemical reduction of ferric $Mb^{III}(H_2O)$. Further, Liu et al. have noted differences in the X-ray crystal structures of *Thermus* cyt ba_3 oxidase reduction products depending on whether X-ray photoreduction or chemical reduction was employed (15); the structure of the active site of the X-ray photoreduced enzyme at 100 K showed retention of the bridging water molecule at the Fe-Cu bimetallic active site, in contrast to the structure of the dithionite-reduced ba_3 that did not show such a bridging water molecule.

In summary, we have successfully generated and cryotrapped a nitrite adduct of ferrous d^6 Mb^{II} at 100 K. This represents the first reported crystal structure of a nitrite adduct of any ferrous mammalian heme protein. Experiments to investigate the thermal stability and reactivity of this $Mb^{II}(ONO)$* complex are underway.

Supplementary Material

Refer to Web version on PubMed Central for supplementary material.

Acknowledgments

Data for this study were measured, in part, at beamline X26-C of the National Synchrotron Light Source (NSLS) at the Brookhaven National Laboratory. Use of the NSLS was supported by the U.S. Department of Energy Office of Basic Energy Sciences, under Contract DE-AC02-98CH10886. We thank Dr. Timothy Sage for alerting us to reference 12.

References

1. Hendgen-Cotta UB, Merx MW, Shiva S, Schmitz J, Becher S, Klare JP, Steinhoff HJ, Goedecke A, Schrader J, Gladwin MT, Kelm M, Rassaf T. Nitrite Reductase Activity of Myoglobin Regulates Respiration and Cellular Viability in Myocardial Ischemia-Reperfusion Injury. Proc Natl Acad Sci USA. 2008; 105:10256–10261. [PubMed: 18632562]
2. van Faassen EE, Babrami S, Feelisch M, Hogg N, Kelm M, Kim-Shapiro DB, Kozlov AV, Li HT, Lundberg JO, Mason R, Nohl H, Rassaf T, Samouilov A, Slama-Schwok A, Shiva S, Vanin AF,

Weitzberg E, Zweier J, Gladwin MT. Nitrite as Regulator of Hypoxic Signaling in Mammalian Physiology. Med Res Rev. 2009; 29:683–741. [PubMed: 19219851]

3. Copeland DM, Soares A, West AH, Richter-Addo GB. Crystal Structures of the Nitrite and Nitric Oxide Complexes of Horse Heart Myoglobin. J Inorg Biochem. 2006; 100:1413–1425. [PubMed: 16777231]
4. Yi J, Heinecke J, Tan H, Ford PC, Richter-Addo GB. The Distal Pocket Histidine Residue in Horse Heart Myoglobin Directs the *O*-Binding Mode of Nitrite to the Heme Iron. J Am Chem Soc. 2009; 131:18119–18128. [PubMed: 19924902]
5. Williams PA, Fulop V, Garman EF, Saunders NFW, Ferguson SJ, Hajdu J. Haem-ligand Switching During Catalysis in Crystals of a Nitrogen-Cycle Enzyme. Nature. 1997; 389:406–412. [PubMed: 9311786]
6. Crane BR, Siegel LM, Getzoff ED. Probing the Catalytic Mechanism of Sulfite Reductase by X-ray Crystallography: Structures of the *Escherichia coli* Hemoprotein in Complex with Substrates, Inhibitors, Intermediates, and Products. Biochemistry. 1997; 36:12120–12137. [PubMed: 9315849]
7. Lukat P, Rudolf M, Stach P, Messerschmidt A, Kroneck PMH, Simon J, Einsle O. Binding and Reduction of Sulfite by Cytochrome *c* Nitrite Reductase. Biochemistry. 2008; 47:2080–2086. [PubMed: 18201106]
8. Polyakov KM, Boyko KM, Tikhonova Tv, Slutsky A, Antipov AN, Zvyagilskaya RA, Popov AN, Bourenkov GP, Lamzin VS, Popov VO. High-Resolution Structural Analysis of a Novel Octaheme Cytochrome c Nitrite Reductase from the Haloalkaliphilic Bacterium *Thioalkalivibrio nitratireducens*. J Mol Biol. 2009; 389:846–862. [PubMed: 19393666]
9. Yi J, Safo MK, Richter-Addo GB. The Nitrite Anion Binds to Human Hemoglobin via the Uncommon *O*-Nitrito Mode. Biochemistry. 2008; 47:8247–8249. [PubMed: 18630930]
10. Beitlich T, Kuhnel K, Schultze-Briese C, Shoeman RL, Schlichting I. Cryoradiolytic Reduction of Crystalline Heme Proteins: Analysis by UV-Vis Spectroscopy and X-ray Crystallography. J Synchrotron Rad. 2007; 14:11–23.
11. Paithankar KS, Owen RL, Garman EF. Absorbed Dose Calculations for Macromolecular Crystals: Improvements to RADDOSE. J Synchrotron Rad. 2009; 16:152–162.
12. Engler N, Ostermann A, Gassmann A, Lamb DC, Prusakov VE, Schott J, Schweitzer-Stenner R, Parak FG. Protein Dynamics in an Intermediate State of Myoglobin: Optical Absorption, Resonance Raman Spectroscopy, and X-Ray Structure Analysis. Biophys J. 2000; 78:2081–2092. [PubMed: 10733986]
13. Reddy KS, Yonetani T, Tsuneshige A, Chance B, Kushkuley B, Stavrov SS, Vanderkooi JM. Infrared Spectroscopy of the Cyanide Complex of Iron(II) Myoglobin and Comparison with Complexes of Microperoxidase and Hemoglobin. Biochemistry. 1996; 35:5562–5570. [PubMed: 8611547]
14. Zahran ZN, Chooback L, Copeland DM, West AH, Richter-Addo GB. Crystal Structures of Manganese- and Cobalt-Substituted Myoglobin in Complex with NO and Nitrite Reveal Unusual Ligand Conformations. J Inorg Biochem. 2008; 102:216–233. [PubMed: 17905436]
15. Liu B, Chen Y, Doukov T, Soltis SM, Stout CD, Fee JA. Combined Microspectrophotometric and Crystallographic Examination of Chemically Reduced and X-ray Radiation-Reduced Forms of Cytochrome ba_3 Oxidase from *Thermus thermophilus*: Structure of the Reduced Form of the Enzyme. Biochemistry. 2009; 48:820–826. [PubMed: 19140675]

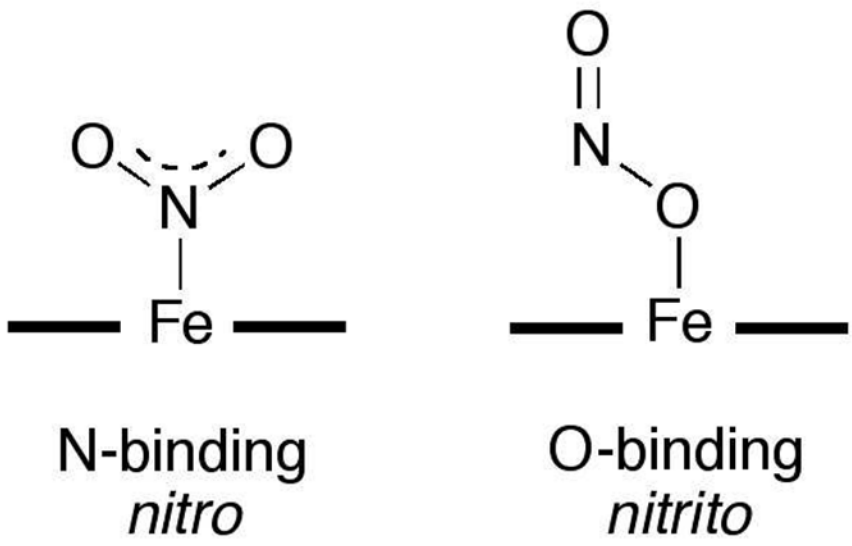

Figure 1.
Heme nitrite binding modes.

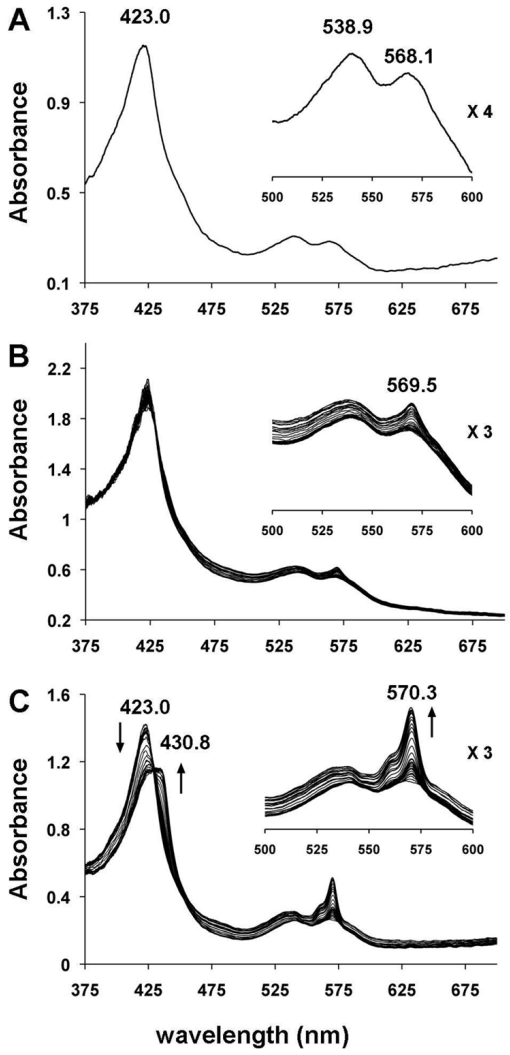

Figure 2.

Single-crystal UV-vis spectra (~25 μm incident light focal spot size) at 100 K of (**A**) ferric Mb^{III}(ONO), (**B**) ferric Mb^{III}(ONO) exposed to low-intensity X-rays over a 95 min period, and (**C**) ferric Mb^{III}(ONO) exposed to high-intensity X-rays over a 50 min period; the first 15 spectra were collected after each image frame (15 s exposure per frame) and the remaining spectra collected after each set of 10 frames.

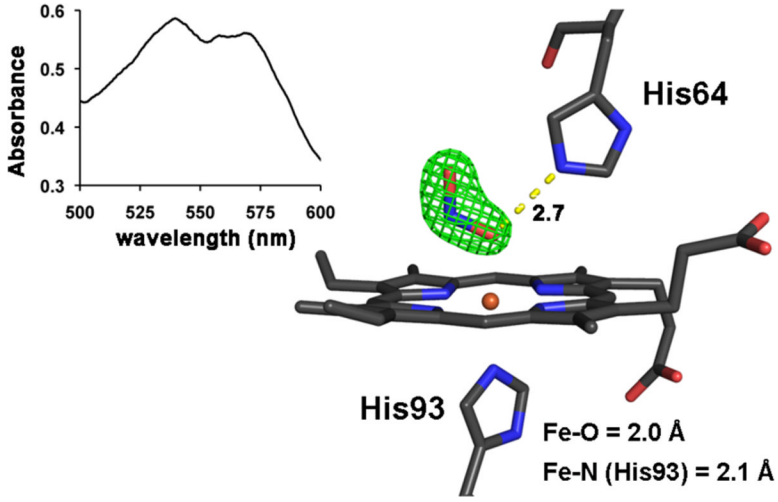

Figure 3.

Left: Single-crystal optical spectrum (500–600 nm region; ~25 μm incident light focal spot size) of a crystal of ferric Mb^{III}(ONO) after 12 h exposure to low-intensity home source X-rays. *Right:* The F_o-F_c omit electron density map (contoured at 5σ) and final model of the heme environment of ferric Mb^{III}(ONO) (1.60 Å resolution structure) after exposure to low-intensity home source X-rays. The bonds to Fe are omitted for clarity, and the hydrogen bond between the nitrito ligand and the distal His64 residue is shown as a yellow dashed line (distance in Å). PDB access code 3LR7.

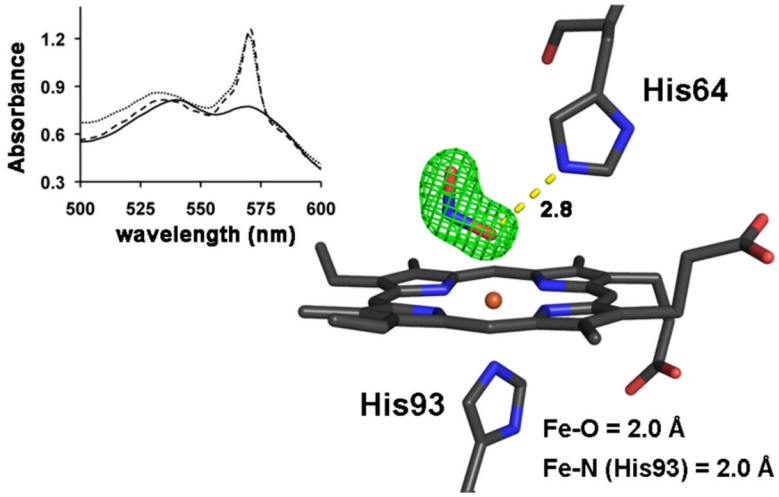

Figure 4.

Left: Single-crystal optical spectra (500–600 nm region; ~25 μm incident light focal spot size) of a crystal of ferric Mb^{III}(ONO) during exposure to high-intensity X-rays. The dark line is the original spectrum before X-ray exposure; the dashed line is the spectrum after exposure of the crystal to X-rays for 161 images at 15s/image; the grey line is the spectrum at the end of data collection (365 images at 15s/image). *Right:* The F_o-F_c omit electron density map (contoured at 5σ) and final model of the heme environment (1.55 Å resolution structure) of the ferrous Mb^{II}(ONO)* product obtained after exposure of the ferric precursor to high-intensity X-rays using the image numbers 161–365 for the structure determination. The bonds to Fe are omitted for clarity, and the H-bond between the nitrito ligand and the distal His64 residue is shown as a yellow dashed line (distance in Å). PDB access code 3LR9. Animations (in avi format) of the correlated crystal rotation-spectroscopy have been deposited with the PDB and as Supporting Information.

Table 1

Data Collection and Refinement Statistics[a]

	Mb^{III}(ONO)	Mb^{II}(ONO)*
Space Group	$P2_1$	$P2_1$
wavelength (Å)	1.5418	1.0000
resoln range (Å)	21.85–1.60	26.74–1.55
unique reflns	15927	17892
completeness	98.0% (96.0)	99.2% (95.3)
I/σ(I)	9.9 (3.0)	15.7 (3.9)
R_{merge} (%)	5.6 (29.8)	4.2 (18.6)
R (R_{free}) (%)	19.3 (22.2)	17.8 (21.0)

[a]The data in brackets refer to the highest resolution shells.